

AD-A063 113

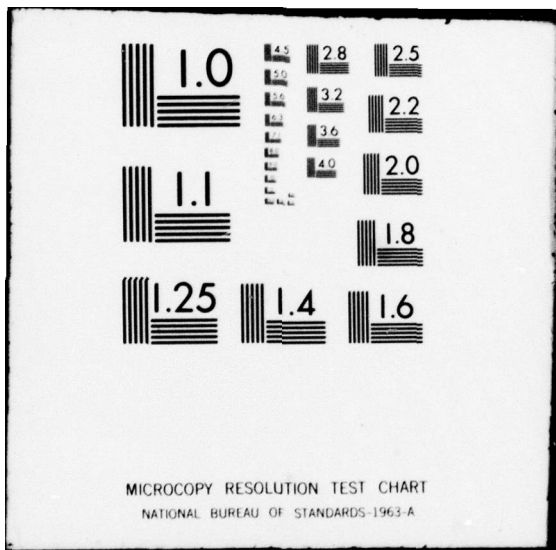
MATHEMATICAL APPLICATIONS GROUP INC ELMSFORD N Y
THE EFFECTS OF AIR AND GROUND COMPOSITION PERTURBATIONS UPON EN--ETC(U)
DEC 78 M BEER, M O COHEN, E S TROUBETZKOY DAAG39-77-C-0020
MR-7061 HDL-CR-78-020-1 NL

UNCLASSIFIED

| OF |
AD
A063 113



END
DATE
FILMED
3-79
DDC



MICROCOPY RESOLUTION TEST CHART
NATIONAL BUREAU OF STANDARDS-1963-A

LEVEL ⁷

J
12

AD A063113

HDL-CR-78-020-1

DECEMBER 1978

The Effects of Air and Ground Composition Perturbations upon
Energy Deposition Rates and Compton Electron Currents from a
Surface Burst

DDC FILE COPY

Prepared by

Mathematical Applications Group, Inc.
3 Westchester Plaza
Elmsford, N. Y. 10523

DDC
RECEIVED
JAN 11 1979
F

Under contract

DAAG39-77-C-0020



U.S. Army Electronics Research
and Development Command
Harry Diamond Laboratories
Adelphi, MD 20783

Approved for public release; distribution unlimited.

79 01 09 049

The findings in this report are not to be construed as an official Department of the Army position unless so designated by other authorized documents.

Citation of manufacturers' or trade names does not constitute an official indorsement or approval of the use thereof.

Destroy this report when it is no longer needed. Do not return it to the originator.

UNCLASSIFIED

SECURITY CLASSIFICATION OF THIS PAGE (When Data Entered)

REPORT DOCUMENTATION PAGE		READ INSTRUCTIONS BEFORE COMPLETING FORM
1. REPORT NUMBER	2. GOVT ACCESSION NO.	3. RECIPIENT'S CATALOG NUMBER
4. TITLE (and Subtitle) 6 THE EFFECTS OF AIR AND GROUND COMPOSITION PERTURBATIONS UPON ENERGY DEPOSITION RATES AND COMPTON ELECTRON CURRENTS FROM A SURFACE BURST		5. TYPE OF REPORT & PERIOD COVERED Final Report Nov. 17, 1976 - Nov. 10, 1978
7. AUTHOR(s) 10 Mendel/Beer, Martin O./Cohen Eugene S./Troubetzkoy		6. PERFORMING ORG. REPORT NUMBER 14 MR-7061
8. PERFORMING ORGANIZATION NAME AND ADDRESS Mathematical Applications Group, Inc. 3 Westchester Plaza Elmsford, New York 10523		9. CONTRACT OR GRANT NUMBER(s) 15 DAAG39-77-C-0020
11. CONTROLLING OFFICE NAME AND ADDRESS Harry Diamond Laboratories 2800 Powder Mill Road Adelphi, Md. 20783		10. PROGRAM ELEMENT, PROJECT, TASK AREA & WORK UNIT NUMBERS 62118A, 1L16218AH75, 12118 H750011 PRON# A17R000402A1A9
12. MONITORING AGENCY NAME & ADDRESS (if different from Controlling Office) 12 38 p.		11. SECURITY CLASS. (of this report) UNCLASSIFIED
16. DISTRIBUTION STATEMENT (of this Report) APPROVED FOR PUBLIC RELEASE; DISTRIBUTION UNLIMITED		12. SECURITY DATE 11 December 1978
17. DISTRIBUTION STATEMENT (of the abstract entered in Block 20, if different from Report) 18 HDL 19 CR-78-020-1		13. NUMBER OF PAGES 38
18. SUPPLEMENTARY NOTES HDL Project No. X757E7 16 1L16218AH75		14. DECLASSIFICATION/DOWNGRADING SCHEDULE
19. KEY WORDS (Continue on reverse side if necessary and identify by block number) Compton Electron Currents Radial, Polar Components Energy Deposition Time Dependence Atmosphere Neutron Source Energy Bands Ground Composition Perturbations SAM-CE Monte Carlo Code		
20. ABSTRACT (Continue on reverse side if necessary and identify by block number) A series of time-dependent Monte Carlo perturbation calculations has been performed to determine, as functions of neutron source energy band, the energy deposition rates and Compton electron sources in the air due to neutron and secondary photon interactions from weapons at a one meter height of burst. Both total value and composition perturbation differences were calculated for atmospheric water volume fractions of 2% and 4%. Nevada test soil was used for the base case		

DD FORM 1 JAN 73 1473 EDITION OF 1 NOV 68 IS OBSOLETE

UNCLASSIFIED

SECURITY CLASSIFICATION OF THIS PAGE (When Data Entered)

390 389

not pay
set

UNCLASSIFIED

SECURITY CLASSIFICATION OF THIS PAGE(When Data Entered)

ground composition. The small perturbations considered were water in air and water, silicon, aluminum and iron in ground. The energy deposition rates and Compton electron sources were determined as functions of time (out to 100-ms local time), in 49 radial and altitude scoring bins surrounding the four isotropic point sources. Answers were obtained for penetrations from 0 to 2.4 km in the horizontal direction and from 0 to 1.5 km above the air-ground interface.

The raw data have been stored on tapes at HDL. Some sample results are presented and described in this report. More analysis is required to obtain further results.

Handwritten checkmark ✓

ACCESS	
NTIS	<input type="checkbox"/>
DOC	<input type="checkbox"/>
BY	DISPER/TOMMY/ASPT/TT/TT/TT/TT
DI	SECRET
A	

UNCLASSIFIED

SECURITY CLASSIFICATION OF THIS PAGE(When Data Entered)

TABLE OF CONTENTS

1. INTRODUCTION. 7

2. COMPUTATIONAL TECHNIQUE 8

 2.1 Basic Procedure. 8

 2.2 Code Modifications for Unperturbed Computations. 8

 2.3 Code Modifications for Perturbed Computations. 10

 2.4 Data Transmittal to Harry Diamond Laboratories 11

3. CALCULATIONAL PROGRAM 12

 3.1 Source Altitude. 12

 3.2 Source Energy Bands. 12

 3.3 Unperturbed Air and Ground Descriptions. 12

 3.4 Perturbations in Air and Ground Compositions 12

 3.4.1 Air Compositions. 12

 3.4.1.1 Water Vapor and Ideal Gas Law 12

 3.4.1.2 Base and Perturbed Air Compositions 17

 3.4.2 Base and Unperturbed Ground Compositions. 17

 3.5 Cross Sections and Response Functions. 17

 3.6 Special Scoring Bins 19

 3.7 Time Bins. 19

 3.8 Importance Sampling. 19

4. DESCRIPTION OF RESULTS. 23

 4.1 Results Presented. 23

 4.2 Time-Integrated Composition Perturbation Results 24

 4.2.1 General Discussion. 24

 4.2.2 Neutron Energy Deposition 24

 4.2.3 Low Energy Neutron Air Gamma Rays 24

 4.2.4 Low Energy Neutron Ground Gamma Rays. 24

 4.2.5 High Energy Neutron Air Gamma Rays. 25

 4.2.6 High Energy Neutron Ground Gamma Rays 25

 4.3 Time Dependent Results 25

5. CONCLUSIONS 35

DISTRIBUTION. 37

LIST OF TABLES

TABLE 1 - Source Energy Band Structure.	13
TABLE 2 - Base Composition and Perturbation Composition Differences for Air	14
TABLE 3 - Base Atomic and Perturbation Composition Differences for Ground.	15
TABLE 4 - Cross Section Data Base	18
TABLE 5 - Additional Subdivision of Selected Regions near Air-Ground Interface	21
TABLE 6 - Time Bin Structure.	22

LIST OF FIGURES

Figure 1 - Basic Source-Detector Geometry
Used in Monte Carlo Calculations. 9

Figure 2 - Description of Scoring Regions. 20

Figure 3 - Neutron Energy Deposition, 1.83 to 2.35 MeV 26

Figure 4 - Gamma Ray Energy Deposition, Low Energy
Neutrons in Air, 1.83 to 2.35 MeV 27

Figure 5 - Gamma Ray Energy Deposition, Low Energy
Neutrons in Ground, 1.83 to 2.35 MeV. 28

Figure 6 - Gamma Ray Energy Deposition, High Energy
Neutrons in Ground, 1.83 to 2.35 MeV. 29

Figure 7 - Neutron Energy Deposition, 8.19 to 15.0 MeV 30

Figure 8 - Gamma Ray Energy Deposition, Low Energy
Neutrons in Air, 8.19 to 15.0 MeV 31

Figure 9 - Gamma Ray Energy Deposition, Low Energy
Neutrons in Ground, 8.19 to 15.0 MeV. 32

Figure 10- Gamma Ray Energy Deposition, High Energy
Neutrons in Air, 8.19 to 15.0 MeV 33

Figure 11- Gamma Ray Energy Deposition, High Energy
Neutrons in Ground, 8.19 to 15.0 MeV. 34

1. INTRODUCTION

Mathematical Applications Group, Inc. (MAGI), has performed a series of time-dependent Monte Carlo perturbation calculations to determine the effects of air and soil variations upon energy deposition rates and Compton electron sources from a surface nuclear burst. These calculations were made with a modified version of the SAM-CE computer program.¹

The source of primary neutrons was an isotropic emitter at a nominal height of one meter. Calculations were performed for contiguous energy bands which, when combined, can reconstitute arbitrary neutron output spectra.

In previous work involving unperturbed air and soil compositions only, dry air was assumed.² In the current work, two separate sets of calculations were performed, the first involving an unperturbed air composition containing 2% water vapor, by volume, and the second involving a composition containing 4% water vapor, by volume. Perturbations in the aluminum, silicon, iron, and moisture content of the ground and the water vapor content of the air were considered.

For both the unperturbed and perturbed compositions, time-dependent energy deposition and Compton currents were determined in 49 radial and altitude (R-Z) scoring bins surrounding a burst point. The atmosphere, for all compositions, was taken to be homogeneous at an assumed density of 1.11 mg/cm³. Answers were obtained for penetrations up to 2.4 km in the horizontal plane and up to 1.5 km above the ground.

-
1. M. O. Cohen, et al., SAM-CE: A Monte Carlo Code for Three Dimensional Neutron, Gamma Ray and Electron Transport (Rev. 5), Mathematical Applications Group, Inc. MR-7052-5 (May 1977).
 2. H. S. Schechter and M. O. Cohen, Energy Deposition Rates and Compton Electron Currents from Low-Altitude Bursts as a Function of Source Energy, Mathematical Applications Group, Inc., HDL-CR- 77-020-1/MR-7054 (November 1977).

2. COMPUTATIONAL TECHNIQUE

2.1 Basic Procedure

The paths of neutrons chosen uniformly from a source energy band were followed through the problem geometry. Energy degradation of the neutrons was accomplished by the usual processes of nuclear elastic and inelastic collisions and absorption. Neutrons degrading to thermal energy were allowed to continue to collide until they were absorbed by target nuclei.

Inelastic collisions and neutron captures leading to gamma ray emission were stored on an interaction tape. The interaction tape supplied the source for secondary gamma rays. Their paths were followed until degradation below 10 keV or until they left the system.

2.2 Code Modifications for Unperturbed Computations

The calculations were performed with a specially modified version of the SAM-CE Monte Carlo program. Alterations to the program, pertinent to the present calculations, include the following:

- a. Time dependence was recorded in local time units defined as time subsequent to the arrival of the uncollided radiation. (For both primary neutron and secondary photon problems, local time zero is defined as the earliest possible arrival of photons.)
- b. Time-dependent energy deposition due to neutron elastic scattering and photon Compton scattering was scored for all spatial regions.
- c. Compton electron sources were scored in radial and polar bins. These are now described:

Figure 1 shows the basic source-detector geometry used in the Monte Carlo calculations.

A point isotropic source is located in the Cartesian coordinate system at $0,0,Z_s$, where Z_s is the source altitude, and a detector is located at X_d, Y_d, Z_d . The X and Y axes define a plane parallel to the ground.

Consider a vector score, \bar{F} , at the detector position. The score, in this case, the average forward range of a Compton electron, can be characterized by its projections along the Cartesian X, Y, and Z axes. This is not the most convenient coordinate system, however. A more convenient coordinate system is defined by three mutually orthogonal vectors \bar{I}_r , \bar{I}_p , and \bar{I}_ϕ , where \bar{I}_r = the radial vector which is colinear to the source-detector axis; \bar{I}_p = the polar vector, where \bar{I}_r and \bar{I}_p define a plane perpendicular to the ground; and \bar{I}_ϕ = the azimuthal vector, which is parallel to the ground.

(It is apparent that, in a homogeneous atmosphere, the algebraic sum of all scores projected onto the azimuthal vector must vanish. Hence, in the Monte Carlo calculations, computer time was not spent projecting individual scores along this vector. The presence of the ground, however, does produce net scores along the polar axis, which would otherwise vanish in an infinite homogeneous air medium.)

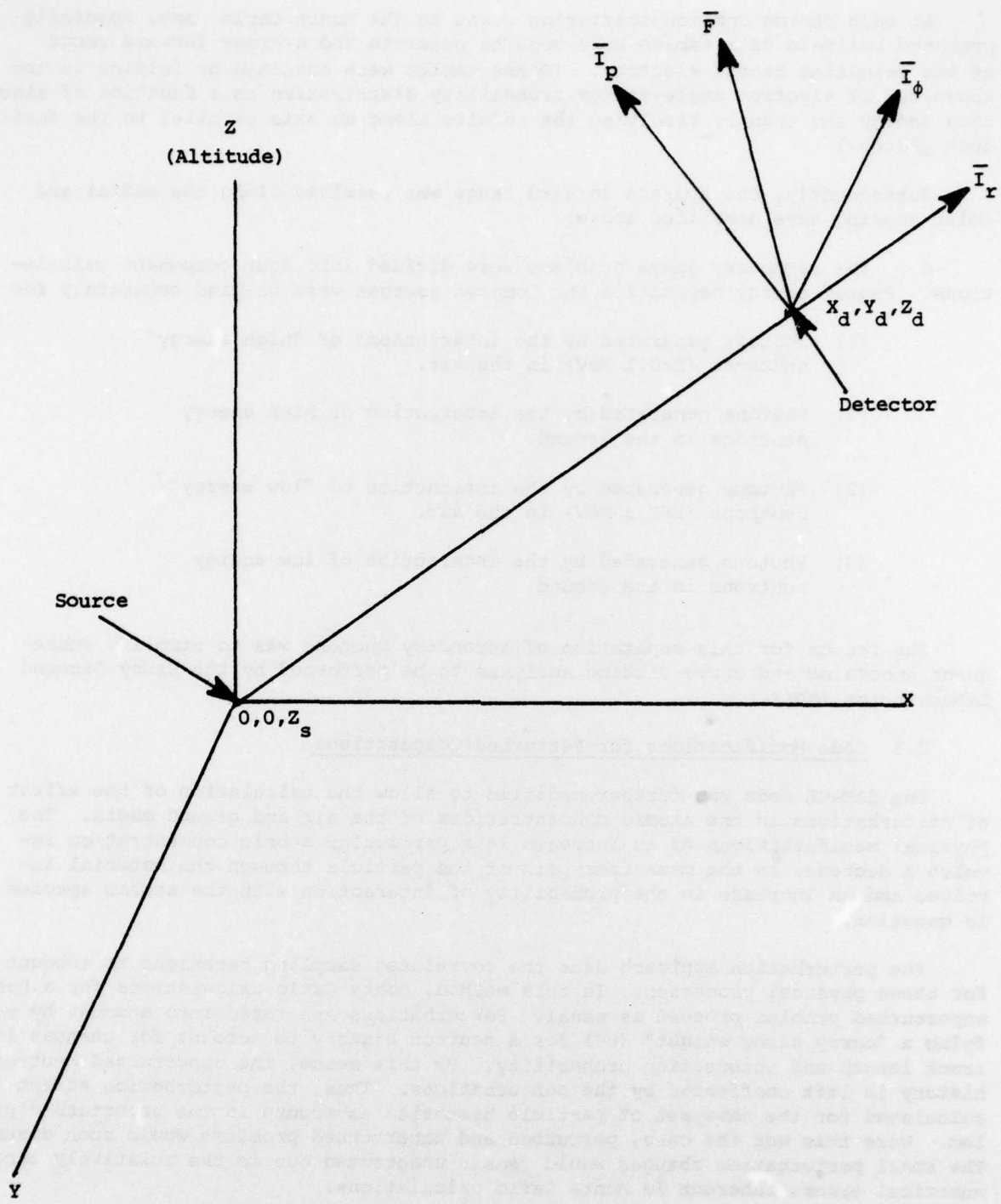


Figure 1 - Basic Source-Detector Geometry Used in Monte Carlo Calculations

At each photon Compton scattering event in the Monte Carlo game, specially prepared built-in data tables were used to generate the average forward range of the resulting recoil electron. (These tables were obtained by folding in the known recoil electron angle-energy probability distribution as a function of electron energy and then by resolving the results along an axis parallel to the incident photon.)

Subsequently, the average forward range was resolved along the radial and polar scoring axes described above.

d. The secondary gamma problems were divided into four component calculations. Photon energy deposition and Compton sources were tallied separately for

- (1) Photons generated by the interactions of "high energy" neutrons ($E > 0.1$ MeV) in the air.
- (2) Photons generated by the interaction of high energy neutrons in the ground.
- (3) Photons generated by the interaction of "low energy" neutrons ($E < 0.1$ MeV) in the air.
- (4) Photons generated by the interaction of low energy neutrons in the ground.

The reason for this separation of secondary photons was to simplify subsequent smoothing and curve-fitting analyses to be performed by the Harry Diamond Laboratories (HDL).

2.3 Code Modifications for Perturbed Computations

The SAM-CE code was further modified to allow the calculation of the effect of perturbations in the atomic concentrations of the air and ground media. The physical manifestations of an increase in a particular atomic concentration involve a decrease in the mean free path of the particle through the material involved and an increase in the probability of interaction with the atomic species in question.

The perturbation approach uses the correlated sampling technique to account for these physical processes. In this method, Monte Carlo calculations for a base, unperturbed problem proceed as usual. Perturbations are taken into account by modifying a "carry along weight" (WC) for a neutron history to account for changes in track length and interaction probability. By this means, the unperturbed neutron history is left unaffected by the perturbations. Thus, the perturbation effect is calculated for the same set of particle histories as occurs in the unperturbed problem. Were this not the case, perturbed and unperturbed problems would soon diverge. The small perturbation changes would remain undetected due to the relatively large numerical errors inherent in Monte Carlo calculations.

Even correlated sampling does not necessarily yield percent errors for perturbation results as small as those for the base problem. As an example, consider the effect of a change in the atomic concentration of iron in ground on neutron energy deposition in an air region for a source located in air. Since only a small proportion of the neutron collisions with atoms occurs with iron, the perturbation

effect may turn out to be very small with large associated statistical errors. On the other hand, a relatively low probability event of a neutron collision with an iron atom may occur and lead to a large and spurious score with a large statistical error. Nevertheless, much better results are obtainable with correlated sampling than without it.

Code modifications included the allowance of carry-along weights for each of up to 10 allowable perturbation problems with associated input and editing requirements.

2.4 Data Transmittal to Harry Diamond Laboratories

The results obtained by MAGI in the course of these calculations were transmitted to HDL for subsequent analyses. In order to simplify the analyses task by HDL, the following were done by MAGI:

a. All scores were written on magnetic tape (in a fixed format) and delivered directly to HDL.

b. For representative source energy bands, computer-generated plots of neutron and secondary photon deposition rates (the latter for all four components)* were provided for selected representative spatial regions.

* If the source neutrons of a high energy component were below the secondary gamma ray production thresholds, the corresponding secondary gamma ray component did not exist.

3. CALCULATIONAL PROGRAM

3.1 Source Altitude

The calculations were performed at ground burst at a nominal 1-m height of burst. This value was selected to maximize ground perturbation effects.

3.2 Source Energy Bands

The source energy band structure is given in Table 1. Previous analyses of the sensitivity of the results to source energy showed that this band structure would be adequate.

3.3 Unperturbed Air and Ground Descriptions

The unperturbed air compositions, as used in the calculations, are given in Table 2. They represent air at a density of 1.11 mg/cm^3 , corresponding to a height above sea level of approximately 900 m. A homogeneous model of the atmosphere was assumed.

The unperturbed ground composition which was used is given in Table 3. It corresponds to soil at a density of 1.70 g/cm^3 .

3.4 Perturbations in Air and Ground Compositions

3.4.1 Air Compositions

3.4.1.1 Water Vapor and Ideal Gas Law

The primary consideration for the transport of neutrons and gamma rays in air is the amount of water vapor in the air. This can be determined by specifying a volume fraction V_w/V . If the partial pressure of the water vapor ratio is given by P_w/P and the molecular number density fraction by n_w/n , it follows from the ideal gas law that

$$V_w/V = P_w/P = n_w/n. \quad (1)$$

-
2. H. S. Schechter and M. O. Cohen, Energy Deposition Rates and Compton Electron Currents from Low-Altitude Bursts as a Function of Source Energy, Mathematical Applications Group, Inc., HDL-CR-77-020-1/MR-7054 (November 1977), 11-12.

TABLE 1

Source Energy Band Structure

Band No.	Energy Interval* (MeV)
1	0.0335 to 0.11
2	0.11 to 0.55
3	0.55 to 1.11
4	1.11 to 1.83
5	1.83 to 2.35
6	2.35 to 4.07
7	4.07 to 6.36
8	6.36 to 8.19
9	8.19 to 15.0

* Uniform (i.e., flat) spectra are assumed within all bands.

TABLE 2

Base Composition and Perturbation Composition
Differences for Air

Problem Type ***	Elements			
	H	N	O	Ar
	Base Case *	Atomic Number Densities (atoms/barn-cm)		
Neutron 2% H ₂ O	9.2308E-7 **	3.5354E-5	9.9917E-6	0
Neutron 4% H ₂ O	1.8462E-6	3.4797E-5	1.0259E-5	0
Gamma Ray 2% H ₂ O	9.2308E-7	3.5522E-5	9.9472E-6	2.1142E-7
Gamma Ray 4% H ₂ O	1.8462E-6	3.4633E-5	1.0215E-5	2.0711E-7
	Perturbation Differences			
Neutron H ₂ O	9.2308E-10	-7.2494E-10	2.6705E-10	0
Gamma Ray H ₂ O	9.2308E-10	-7.2152E-10	2.6795E-10	-4.3148E-12

* Air density = 1.11 mg/cm³

** Read 9.2308 x 10⁻⁷ atoms/barn-cm.

*** Neutron and gamma ray problems are slightly different due to exclusion of argon for neutron problem.

TABLE 3

Base Atomic and Perturbation Composition Differences for Ground*

Problem Type	Elements				
	H	O	Al	Si	Fe
	Base Case Atom Number Densities (atoms/barn-cm)				
All Base Cases	9.577E-3**	3.408E-2	4.785E-3	1.137E-2	3.667E-4
	Perturbation Differences				
Fe	-1.9545E-7	-6.9551E-7	-9.7653E-8	-2.3204E-7	3.667E-7
Si	-4.3406E-6	-1.5446E-5	-2.1687E-6	1.137E-5	-1.662E-7
Al	-1.3818E-6	-4.9172E-6	4.785E-6	-1.6405E-6	-5.2908E-8
H ₂ O	9.577E-6	2.0939E-6	-4.4018E-7	-1.0459E-6	-3.3733E-8

*Ground density = 1.70 g/cm³

**Read 9.577 x 10⁻³ atoms/barn-cm.

The atomic number densities for air are obtained in the following manner. For a density ρ of mixed air and water vapor, ρ_w is defined as the water vapor weight density at the pressure and temperature of the air. Similarly, ρ_a is the weight density of air alone. Then

$$\rho = \rho_w (V_w/V) + \rho_a (1 - V_w/V). \quad (2)$$

The ratio of densities is given by

$$\rho_a / \rho_w = A_w / A_a, \quad (3)$$

where A_w and A_a are the molecular weights for air and water respectively. For the 1967 Standard Atmosphere (a close approximation to the composition considered), the ratio is equal to 1.60776. From Equations (2) and (3) we find

$$\rho = \rho_a [(A_w/A_a) (V_w/V) + (1 - V_w/V)], \quad (4)$$

with a similar expression for ρ in terms of ρ_w . The mass density of water vapor is $\rho_w V_w/V$. If this is multiplied by 2 and by Avogadro's number (N_0) and divided by A_w , we obtain the hydrogen atomic number density:

$$n_{Hw} = 2N_0 H / A_w, \quad (5)$$

where

$$H = \rho (V_w/V) / [1 - (1 - \frac{A_w}{A_a}) V_w/V]. \quad (6)$$

For the Standard Atmosphere $2N_0/A_w = 0.04158$ and $(1 - A_w/A_a) = 0.3781$. Oxygen in water, now is $1/2 n_{Hw}$.

For the different elements of air, we obtain

$$n_i = n_{i0} F / \rho_a, \quad (7)$$

where n_{i0} is the atomic number density for air alone and

$$F = \rho (1 - V_w/V) / [(1 - A_w/A_a) V_w/V]. \quad (8)$$

One can also obtain expressions for linear perturbations Δ in the volume fraction by expanding F and H to first order in Δ to obtain

$$\Delta H = -\Delta F = \rho \Delta / [(1 - A_w/A_a) V_w/V]. \quad (9)$$

3.4.1.2 Base and Perturbed Air Compositions

The first of the base air compositions was chosen to obtain a 2% volume fraction for water vapor. This is close to the saturated water vapor volume at the Standard Atmosphere sea level temperature of 15°C. This amount of water vapor taken over a distance of 2 km corresponds to 2 mean free paths for 100-keV neutrons compared to 37 mean free paths for air. The 4% change in mean free path leads to only small changes in the neutron importance function. This can be ignored in any practical Monte Carlo problem.

The linear perturbation involved the addition of 0.002% water vapor by volume, i.e., a 0.1% increase in water vapor from the base problem. A second base problem involved a 4% volume fraction for water vapor. The same composition perturbations were used with this problem as for the 2% water vapor case.

Atomic concentrations for the base problem and perturbed problems are given in Table 2 for a dry air mass density of 1.11 mg/cm³. Since the original problem of neutron transport in dry air was run without argon, whereas the gamma ray transport problem included argon (the total number of molecules was held constant), separate tabulations are given for neutrons and for gamma rays.

3.4.2 Base and Unperturbed Ground Compositions

The base ground composition in Table 3 represents dry Nevada test soil. It is chosen to include 2 weight percent iron. (This amount of iron is close to that actually occurring in Nevada test soil.) Iron is important to include because of its high thermal capture cross section with subsequent emission of high energy gamma rays.

Carbon, on the other hand, is not included in the base composition. It is not found in Nevada test soil. It does occur in clay soils with an atomic abundance that is lower than oxygen by a factor greater than three. It has a negligible thermal capture cross section, a high threshold for inelastic scatter (4.8 MeV), and its downscattering is small compared to hydrogen. Finally, minor elements, e.g., calcium, are ignored due to their low concentrations in sand and clay soils.

The perturbation composition differences for ground are also shown in Table 3. Small linear perturbations alone are considered for each of the elements with the exception of hydrogen. It is expected that, as long as ground density (1.7 g/cm³) is kept constant, a change in concentration of each of these elements should have only minor effects on neutron and gamma ray transport. The major effect, gamma ray emission, should vary linearly with atomic concentration for all elements except hydrogen.

3.5 Cross Sections and Response Functions

The cross section data base for the computations is given in Table 4. The average range data for Compton electrons, referred to in Section 2, were developed by the authors after consultation with various experts in the field.

TABLE 4

Cross Section Data Base

Element	Neutron Transport and Photon Production Data	Photon Transport Data
Aluminum	ENDF/IV-1193	ENDF/B as dis- seminated by RSIC as Tape DLC-7 D
Hydrogen	ENDF/IV-1269	
Iron	DNA 4180-Mod 2	
Nitrogen	DNA 4133-Mod 4	
Oxygen	ENDF/IV-1276	(All elements including argon)
Silicon	DNA 4151-Mod 2	

3.6 Special Scoring Bins

The atmosphere was divided into stacked and concentric cylinders for scoring₂ and importance sampling (see Section 3.8). The spatial mesh was 300 m (33.3 g/cm²). A finer subdivision of the atmosphere, however, was used closer to the source.

Figure 2 shows the spacing of the scoring regions and the identifying region number associated with each scoring bin. (The unlabeled regions were present in the Monte Carlo calculations for backscattering only.)

In order to investigate the behavior of the scored quantities near the air-ground interface, regions 2, 4, 10, and 12 were further subdivided as shown in Table 5.

3.7 Time Bins

The primary neutron and secondary photon scores were obtained in local time bins out to a 100 millisecond time cutoff. The local time structure is given in Table 6.

3.8 Importance Sampling

The problems to be solved involved difficult Monte Carlo importance sampling situations. Answers were required, with low statistical uncertainties, over many regions of a large multidimensioned phase space. Some of the techniques used to ensure adequate solutions included the following:

a. Energy importance sampling to discriminate against low energy neutron collisions which would be unlikely to generate secondary photons.

b. Spatial importance sampling to generate a sufficient number of neutron high energy interactions at shallow penetrations (since the photons which they generate dominate the early temporal ranges).

c. Spatial importance sampling to obtain adequate solutions at the deep penetrations and to "push" a sufficient number of neutron events towards the ground and towards the special subdivided volumes of Table 5.

d. Directional importance sampling to discriminate against ground-generated photons initially headed downwards deeper into the ground.

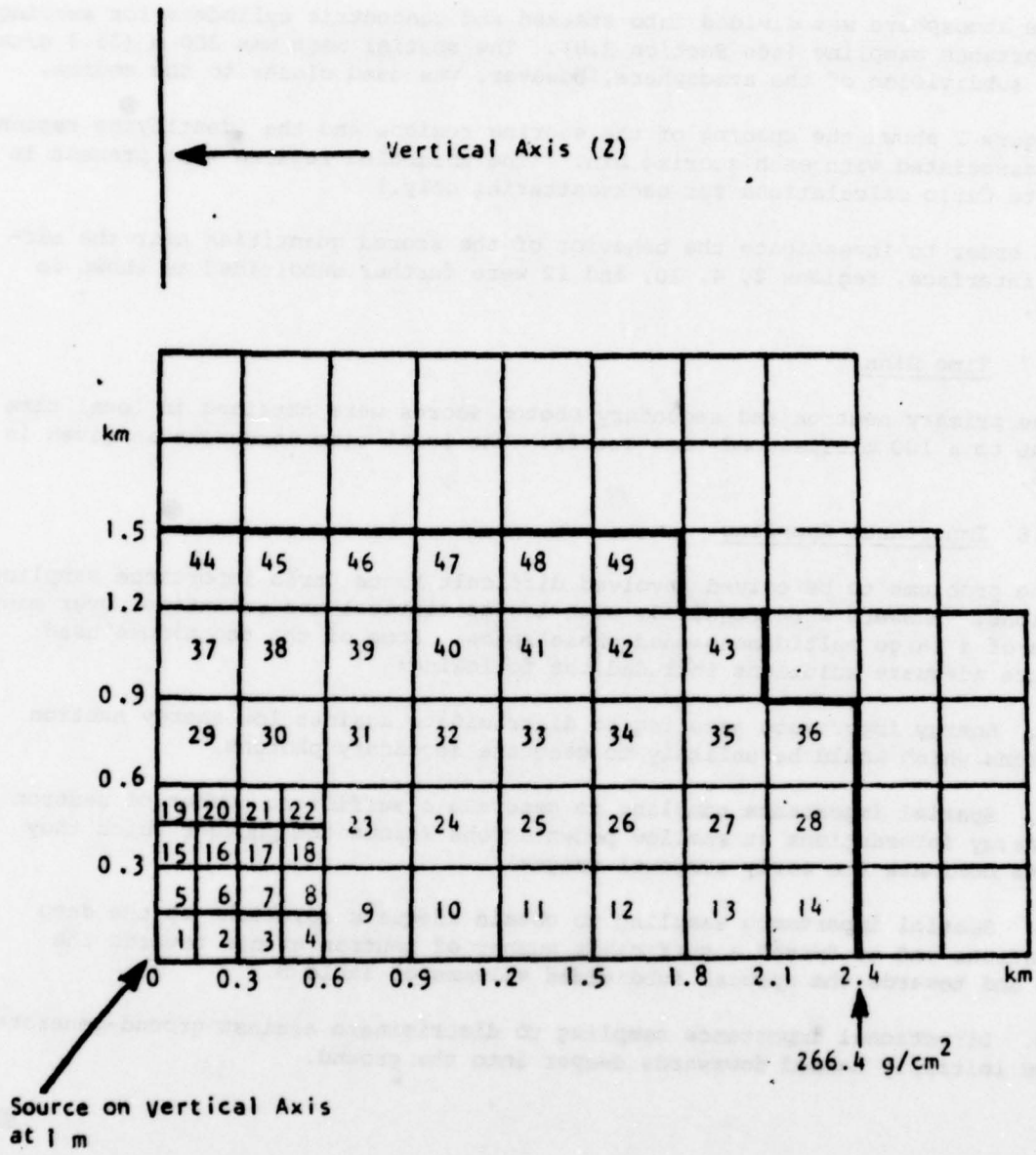


Figure 2 - Description of Scoring Regions

TABLE 5

Additional Subdivision of Selected Regions
near Air-Ground Interface

<u>Nominal Region</u> (refer to Fig. 2)	<u>Subdivisions</u> (Region No.)	<u>Altitude Range</u> (m)
2	50	0 to 25
	51	25 to 50
	52	50 to 100
	2	100 to 150
4	53	0 to 25
	54	25 to 50
	55	50 to 100
	4	100 to 150
10	56	0 to 25
	57	25 to 50
	58	50 to 100
	59	100 to 150
	10	150 to 300
12	60	0 to 25
	61	25 to 50
	62	50 to 100
	63	100 to 150
	12	150 to 300

TABLE 6

Time Bin Structure

Time Bin	Time Interval (s)
1	(0 to 0.100) E-6
2	(0.100 to 0.215) E-6*
3	(0.215 to 0.464) E-6
4	(0.464 to 1.00) E-6
5	(1.00 to 2.15) E-6
6	(2.15 to 4.64) E-6
7	(4.64 to 10.0) E-6
8	(10.0 to 21.5) E-6
9	(21.5 to 46.4) E-6
10	(46.4 to 100.0) E-6
11	(0.100 to 0.215) E-3
12	(0.215 to 0.464) E-3
13	(0.464 to 1.00) E-3
14	(1.00 to 2.15) E-3
15	(2.15 to 4.64) E-3
16	(4.64 to 10.0) E-3
17	(10.0 to 21.5) E-3
18	(21.5 to 46.4) E-3
19	(46.4 to 100.0) E-3

* Read 0.100×10^{-6} to 0.215×10^{-6} s.

4. DESCRIPTION OF RESULTS

4.1 Results Presented

The final results presented in this report are sharply limited for the following reasons:

a. The primary objectives of the studies were to determine energy deposition rates and Compton current sources for both unperturbed problems and composition perturbation differences in the prescribed phase space bins and to forward these raw data to HDL for subsequent smoothing and curve-fitting analyses. These objectives were met, and results for each source band have been delivered by MAGI to HDL as formatted output on magnetic tape.

b. The perturbation difference results form a vast body of new data that require detailed study before curve-fitting methods can be applied in a profitable manner. As discussed previously, the correlated sampling methodology, which was utilized, generally yields lower errors than occur with ordinary Monte Carlo methods. Nevertheless, some of the perturbation difference results involve large errors which require further spatial or temporal averaging or both before quantitative (and, in some cases, qualitative) trends become apparent.

c. Much of the qualitative analyses for the previous study, involving fission and 14-MeV sources,³ apply to the unperturbed band-source results of this study as well. These include

- (1) General temporal shapes of the neutron and four photon components of the energy deposition curves.
- (2) General temporal shapes of the four photon components of the radial and polar Compton current sources.
- (3) Air-ground interface effects.
- (4) Range effects on each of the above.

Hence, for such analyses, the reader is referred to the previous work.³ However, in the sections which follow, some of the salient new qualitative results for composition perturbation effects are presented.

3. M. O. Cohen, H. S. Schechter, and H. A. Steinberg, Time-Dependent Energy Deposition and Compton Electron Currents from Three Selected Low-Altitude Bursts, Mathematical Applications Group, Inc., HDL-CR-76-029-1/MR-7048 (August 1976).

4.2 Time-Integrated Composition Perturbation Results

4.2.1 General Discussion

The following discussion of qualitative effects for energy deposition is based on a brief analysis of some of the data from several of the energy bands for the cases of 2% and 4% (by volume) of water vapor in air. It is subject to any changes that may occur in any future complete analysis of the data.

In the analysis, a parameter, R , the ratio of difference in energy deposition to difference in composition change, is often utilized as a qualitative measure of an effect. No attempt to assess the linearity assumption of this analysis has been made. Such an assessment must await a more complete review of the data.

The discussion is given for elastic scattering neutron energy deposition and gamma ray energy deposition due to the four way split obtained from the division of secondary gamma rays into those born in air or ground and those due to neutron with energy greater than or less than 0.1 MeV. (The 0.1 MeV boundary serves to separate inelastic gamma rays from the neutron capture gamma rays (due to low energy neutrons)).

4.2.2 Neutron Energy Deposition

The most important effect on neutron energy deposition in air regions involves perturbation differences for water in air and ground. A small increase of moisture in air leads to a small positive effect close in to the source and an increasingly negative effect further away. The R value reaches a negative maximum of -0.4. Evidently, hydrogen in air is quite effective in slowing down neutrons in air. On the other hand, a small increase of water density in the ground leads to an R value of about -0.1 near the source and negative values close to zero further away.

4.2.3 Low Energy Neutron Air Gamma Rays

A small increase of water in air leads to an R value close to zero near the source. A negative R value of ~ -0.2 seems to occur far from the source. This effect can be attributed to the increased hydrogen in air causing neutron slowing down and subsequent capture and gamma ray production nearer to the source than otherwise occurs. Comparison of total energy deposition for 2% and 4% moisture in air does not indicate any strong trend. Any true trend cannot be observed due to the statistical errors inherent in the two Monte Carlo problems.

No clear trend was found for a small increase of water in ground. However, R is quite small, i.e., $|R| < 0.1$.

4.2.4 Low Energy Neutron Ground Gamma Rays

A small increase of water in air leads to a small negative effect. Near ground, R is found to be approximately -0.1.

The effect of water in ground was not clearly established from this cursory examination.

An interesting effect is noted for a small increase in iron in ground. R is found to be positive and generally in the range 0.2-0.3. This large effect can be attributed to the high capture cross section of iron and to the relatively high properties of penetrating high energy gamma rays emitted.

If a linear effect is assumed, these numbers extrapolate to an estimated increase in gamma ray energy deposition due to low energy neutron capture in ground of 30-50% for German clay, 90-130% for basalt, and 110-160% for Hawaiian clay.

Finally, an increase in the silicon content of the ground leads to a positive R value in the range of 0.1-0.3.

4.2.5 High Energy Neutron Air Gamma Rays

A small increase of either water in air or water, iron, silicon, or aluminum in ground leads to a small negative R value. The largest effect is found for water in air. Even for this case, the R value is negative and has a magnitude of $-0.1 < R < 0$.

4.2.6 High Energy Neutron Ground Gamma Rays

The addition of water to ground is found to lead to negative R values in the range -0.1 to -0.3. The effect of aluminum and silicon added to ground seems to depend on the neutron energy. Lower neutron energies (but above the inelastic threshold) seem to lead to possibly high R values for silicon (up to 1.0). Higher neutron energies lead to positive R values for aluminum. This effect must be examined much more carefully before valid conclusions can be drawn.

4.3 Time Dependent Results

The Monte Carlo calculations generated a very large volume of information regarding time-dependent results. The results must await analysis at some future time.

In this report, we remain content to give sample plots of neutron energy deposition and the four components of gamma ray energy deposition for region 11 for 4% H₂O in air for two neutron energy bands, 1.83-2.35 and 8.19-15.0 MeV.

In Figures 3-12, the letter Z refers to the zeroth or base case energy deposition. Letters B, C, D, E, and F give positive energy differences (where they occur) relative to the base case, respectively, for the five perturbations: B - aluminum (ground), C - iron (ground), D - silicon (ground), E - water (ground), and F - water (air). The letters G, H, I, J, and K represent negative perturbation differences (where they occur) relative to the base corresponding, respectively, to the letters B, C, D, E, and F. The differences scale is 10^6 times the absolute scale. Statistics are not given for the neutron energy deposition. For gamma energy deposition, a number is given which represents the standard deviation. i.e., % standard deviation/10. For the 1.83-2.35 MeV band, all source neutrons are below the threshold energy for the production of the high energy air component of the secondary gamma rays. Hence, there is no figure drawn for this component.

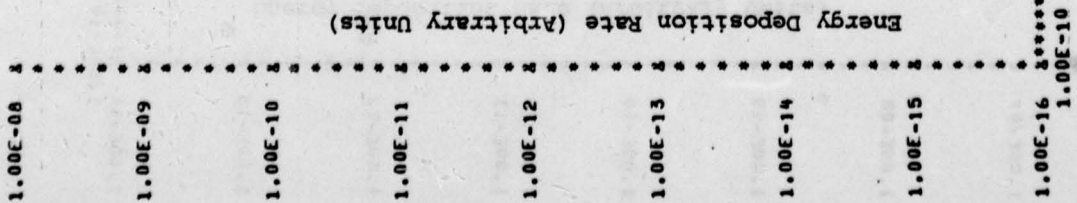
F99F

E666E
E666D99J99J
1777I
6A88G 099I999I J55J

655G K999K
C999C G99G J99H44J999J
F99H777H K999K
H88H 199C77C
F99F
C99C 1999I
K99D9969996

F99F

Z99Z Z33Z
* * Z22Z11Z11Z
* * Z777Z77Z
* * Z111Z



TIME
P/D SCALE= 0.1E+07
GAMMA RAY ENERGY DEPOSITION, ITMOPT 1 4PC H20
REGION 11
INTEGRAL= 0.1231E-11

Figure 4 - Gamma Ray Energy Deposition, Low Energy Neutrons in Air, 1.83-2.35 Mev

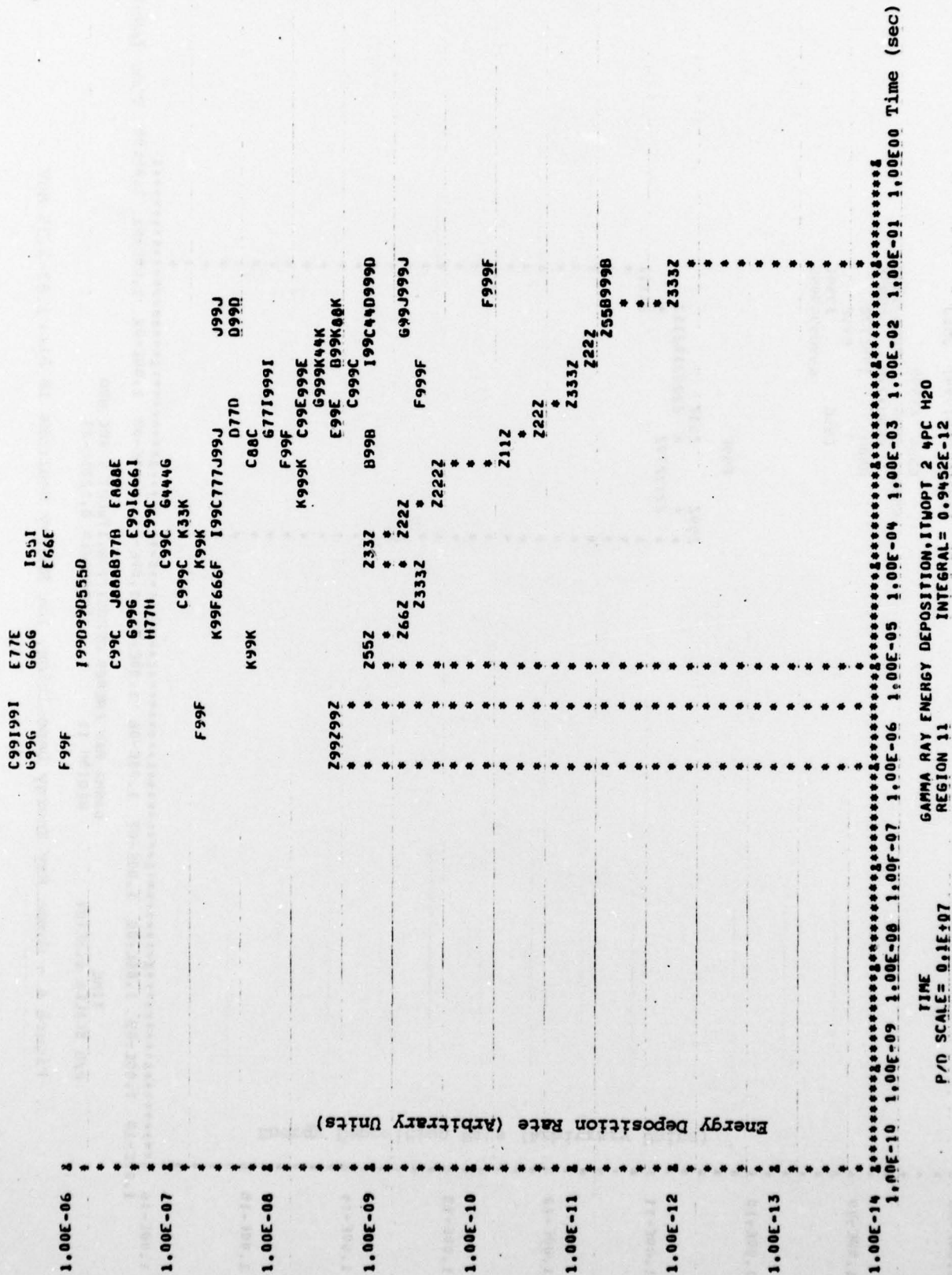
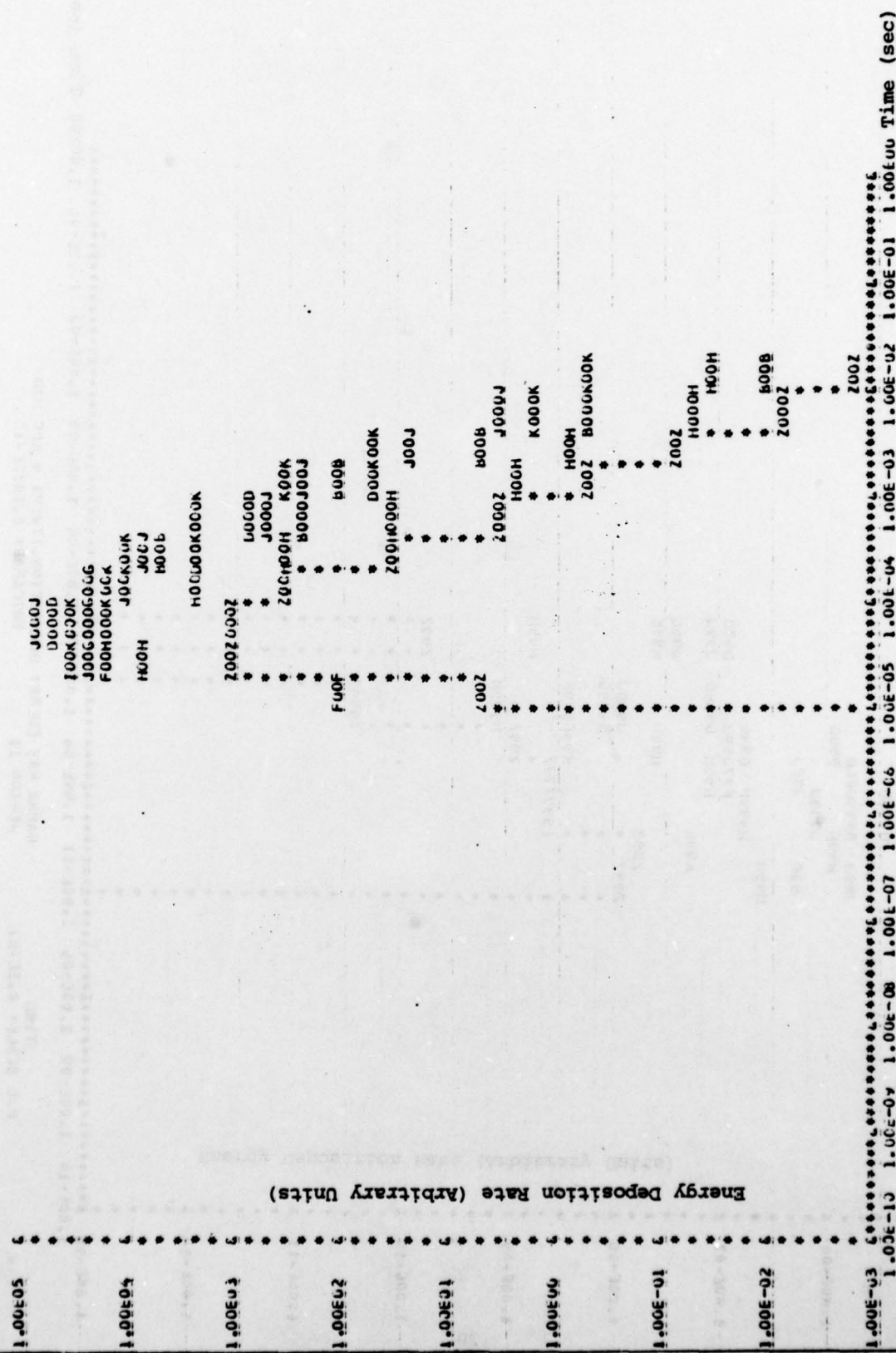


Figure 5 - Gamma Ray Energy Deposition, Low Energy Neutrons in Ground, 1.83-2.35 MeV



TIME SCALE = 0.1E+07
 NEUTRON ENERGY DEPOSITION REGION 11
 INTEGRAL = 0.1483E+00

Figure 7 - Neutron Energy Deposition, 8.19-15.0 MeV

5. CONCLUSIONS

The Harry Diamond Laboratories required, by neutron source energy band, the energy deposition rates and the Compton currents due to a one meter high burst. The spatial range was out to 2.4 km in the horizontal direction and from 0 to 1.5 km above the air-ground interface. The temporal range was out to 100 ms. Through the careful use of importance sampling and some special coding, MAGI has used the SAM-CE Monte Carlo program to generate the raw data in the important phase space regions. Both total value and perturbation differences were calculated for atmospheric water volume fractions of 2% and 4%. Nevada test soil was used for the base case. The small perturbations included water in air and water, silicon, aluminum, and iron in ground. These data have been forwarded to HDL for subsequent processing (see below). Typical raw data results have been presented (for energy deposition) in Section 4 to highlight the more important trends.

It should be noted that the ultimate goal of this program is the smoothing and analytic fitting of the MAGI data. It is believed that an intermediate step would be useful before this goal can be achieved. It may be necessary to average data spatially or temporally to obtain sufficient statistical accuracy for any future fitting procedure.

DISTRIBUTION LIST

	<u>COPIES</u>
Defense Documentation Center ATTN: DDC-TCA Cameron Station, Building 5 Alexandria, Va. 22314	12
Director Defense Nuclear Agency Washington, D.C. 20305	
ATTN: STSI	1
ATTN: STRA	1
ATTN: STTL	1
ATTN: RAEV (Mr. George Baker)	1
Commander Harry Diamond Laboratories 2800 Powder Mill Road Adelphi, Md. 20783	
ATTN: DELHD-TI, Tech. Lib.	3
ATTN: DELHD-EMC, William T. Wyatt, Jr.	3
ATTN: DELHD-EMC, Daniel J. Spohn	1
ATTN: DELHD-NP, Francis N. Wimeritz	1
ATTN: DELHD-TIC	1
ATTN: DELHD-ASA (Record Copy)	1
ATTN: DELHD-TR	1
Director US Army Ballistic Research Laboratories ATTN: DRXBR-AM, Dr. N. E. Banks Aberdeen Proving Ground, Md. 21005	1
Commander Naval Surface Weapons Center White Oak Laboratory Silver Spring, Md. 20910	
ATTN: Code WA-501, Navy Nuc. Prgms. Offc.	1
ATTN: Code WA-50, Dr. John H. Malloy	1
ATTN: Code WX-21, Tech. Lib.	1
Commander Air Force Weapons Laboratory, AFSC Kirtland Air Force Base, NM 87117	
ATTN: ELT, Dr. William Page	2
ATTN: SUL, Tech. Lib.	1
Los Alamos Scientific Laboratory ATTN: Document Control for Dr. John S. Malik Los Alamos, NM 87544	1

DISTRIBUTION LIST (continued)

	<u>COPIES</u>
Mission Research Corporation P. O. Drawer 719 Santa Barbara, Ca. 93102 ATTN: Dr. Conrad L. Longmire	2
ATTN: Technical Library	1
R&D Associates ATTN: R. R. Schaefer	1
P. O. Box 3580 Santa Monica, Ca. 90403	
General Electric Company TEMPO-Center for Advanced Studies ATTN: DASIAC	1
816 State Street Santa Barbara, Ca. 93102	
JAYCOR, Inc. ATTN: William A. Radasky	1
1401 Camino Del Mar Del Mar, Ca. 92014	
Mathematical Applications Group, Inc. ATTN: M. O. Cohen	2
3 Westchester Plaza Elmsford, N. Y. 10523	
Dr. Paul N. Stevens Dept. of Nuclear Engineering University of Tennessee Knoxville, Tn. 22193	1
Radiation Shielding Information Center Oak Ridge National Laboratory Post Office Box X Oak Ridge, Tn. 37830	2